

**Earth system model
simulations of the
LGM**

R. J. Matear et al.

This discussion paper is/has been under review for the journal *Climate of the Past* (CP).
Please refer to the corresponding final paper in CP if available.

The simulated climate of the Last Glacial Maximum and the insights into the global carbon cycle

R. J. Matear¹, A. Lenton¹, D. Etheridge², and S. J. Phipps³

¹CSIRO Oceans and Atmosphere, CSIRO Marine Laboratories, G.P.O. Box 1538, Hobart, Tasmania, Australia

²CSIRO Marine Research, Aspendale, Victoria, Australia

³Climate Research Centre and the ARC Centre of Excellence for Climate System Science, University of New South Wales, Sydney NSW, Australia

Received: 20 February 2015 – Accepted: 11 March 2015 – Published: 31 March 2015

Correspondence to: R. J. Matear (richard.matear@csiro.au)

Published by Copernicus Publications on behalf of the European Geosciences Union.

Title Page

Abstract

Introduction

Conclusions

References

Tables

Figures



Back

Close

Full Screen / Esc

Printer-friendly Version

Interactive Discussion



Abstract

Global climate models (GCMs) provide an important tool for simulating the earth's climate. Here we present a GCM simulation of the climate of the Last Glacial Maximum (LGM), which was obtained by setting atmospheric greenhouse gas concentrations and the earth's orbital parameters to the values which prevailed at 21 000 years before present (BP). During the LGM, we simulate a significant cooling of the ocean and a dramatic expansion of the sea-ice extent. This behaviour agrees with reconstructions from paleoclimate archives. In the ocean, the LGM simulation produces a significant redistribution of dissolved oxygen and carbon. The oxygen levels rise and the volume of anoxic water declines by more than 50 %, which is consistent with paleoclimate reconstructions of denitrification. The simulated LGM climate also stores more carbon in the deep ocean (below 2000 m), but with a reduced atmospheric CO₂ level the total carbon stored in the ocean declines by 600 Pg C. The LGM ocean circulation preconditions the ocean to store carbon in the deep; however, the ocean circulation and sea-ice changes are insufficient alone to increase the total carbon stored in the ocean and modifications to the ocean biogeochemical cycles are required. With modifications to organic and inorganic carbon export and organic carbon remineralization one can increase ocean carbon storage (240 Pg C) to a level that is sufficient to explain the reduction in atmospheric and land carbon during the LGM (520 ± 400 Pg C). With the modified biogeochemical cycling in the ocean, the simulated aragonite lysocline depth and dissolved oxygen become more consistent with paleo-reconstructions.

1 Introduction

Over recent glacial cycles, global temperature and atmospheric CO₂ are highly correlated with an 80–100 ppm lower atmospheric CO₂ concentration during colder glacial cycles (Sigman et al., 2010). The atmospheric CO₂ reduction during the glacial periods provides a global climate forcing that may help explain the cooling during glacial peri-

CPD

11, 1093–1142, 2015

Earth system model simulations of the LGM

R. J. Matear et al.

Title Page

Abstract

Introduction

Conclusions

References

Tables

Figures



Back

Close

Full Screen / Esc

Printer-friendly Version

Interactive Discussion



**Earth system model
simulations of the
LGM**

R. J. Matear et al.

[Title Page](#)[Abstract](#)[Introduction](#)[Conclusions](#)[References](#)[Tables](#)[Figures](#)[Back](#)[Close](#)[Full Screen / Esc](#)[Printer-friendly Version](#)[Interactive Discussion](#)

ods. However, the cause of the reduction in CO₂ during glacial periods remains a fundamental unresolved question for earth system science (Archer et al., 2000; Brovkin et al., 2007). Given the much larger carbon storage in the ocean than either the land or the atmosphere, it is widely accepted that the ocean must dominate glacial/interglacial changes in atmospheric CO₂ (Peacock et al., 2006).

The most promising explanations for the atmospheric CO₂ decrease involve ocean biogeochemistry and its interaction with ocean circulation (Sigman et al., 2010). Potential causes include increased iron supply to the ocean (Martin, 1990), increased sea-ice cover (Stephens and Keeling, 2000), changes in the availability of nutrients (Broecker and Henderson, 1998), circulation changes (Toggweiler and Russell, 2006), increased ocean alkalinity (Archer et al., 2000) and some combination of all the above. These explanations for the reduction in atmospheric CO₂ during glacial periods identify the importance of the ocean circulation and its effect on the global efficiency of the biological pump.

The response of the earth system to the conditions of the Last Glacial Maximum (LGM) provide a useful assessment of our ability to simulate the earth's climate (Falkowski et al., 2000). We use a global climate model (GCM) to simulate the conditions during the LGM. Our study assesses the ability of the GCM to simulate the LGM climate and then explores how the simulated ocean state during the LGM affects the carbon content and distribution in the ocean. Following Tagliabue et al. (2009), we employ global 3-D climate and ocean models to enable a spatial assessment of the simulated behaviour. Using our simulated LGM ocean state, we provide a new perspective on the mechanisms responsible for the 80–100 ppm drawdown in atmospheric CO₂ during glacial cycles. The simulations also provide an additional perspective on the distribution of biogeochemical (BGC) tracers in the ocean, which can be used to assess the simulated LGM climate, and the changes in oxygen concentrations and ocean acidification.

2 Model and experiments

The model simulations were performed with the MK3L modelling system (Phipps et al., 2011, 2012), which includes atmosphere–land–sea-ice and ocean components with a simple biogeochemical module embedded in the ocean model (Matear and Lenton, 2014). The horizontal resolution of the atmosphere–land–sea-ice module is $5.6^\circ \times 3.2^\circ$ east–west and north–south respectively, with 18 vertical levels. The ocean module has a horizontal resolution of $2.8^\circ \times 1.6^\circ$ with 21 vertical levels. The modelling system is flexible and simulations of atmosphere, land, sea-ice and ocean components can be done either separately or in coupled mode. For this study, we used both coupled and ocean-only simulations. A description of the physical modelling system is presented in Phipps et al. (2011).

The Holocene climate (HC) was obtained by integrating the coupled model for 5000 years using an atmospheric CO_2 value of 280 ppm and present-day orbital parameters. The LGM climate was obtained by setting the orbital parameters to the conditions 21 kaBP and the equivalent atmospheric CO_2 to 167 ppm. The coupled system was then integrated to quasi-equilibrium (5000 years). The equivalent CO_2 was reduced to 167 ppm following the Paleo Modelling Inter-comparison Project 2 (PMIP2) experiment design to account for the reduction in $\text{CO}_2/\text{CH}_4/\text{N}_2\text{O}$ concentration from the HC values of 280 ppm/760 ppb/270 ppb to the LGM values of 185 ppm/350 ppb/200 ppb (see <http://pmip2.lsce.ipsl.fr/>). In the LGM simulation, the atmospheric CO_2 was prescribed and the climate state was obtained without considering the feedback from the ocean.

The PMIP2 experimental design for a LGM simulation prescribes changes in greenhouse gases and orbital parameters, which we applied. Changes in ice sheet extent, topography and coastline, however, were not applied in our simulations, hence our simulation could be described as being a “simplified version” of PMIP2 experimental design. While we do not take into account the topographic effects of increased land ice, the model is nonetheless capable of simulating a shift in the ice-albedo feedbacks

CPD

11, 1093–1142, 2015

Earth system model simulations of the LGM

R. J. Matear et al.

Title Page

Abstract

Introduction

Conclusions

References

Tables

Figures



Back

Close

Full Screen / Esc

Printer-friendly Version

Interactive Discussion



differ between the HC and LGM climates with a fixed ocean BGC parameterization. Finally, we explore how modifying the BGC parameterization alters the ocean carbon storage and key ocean BGC fields like dissolved oxygen and aragonite saturation state.

3.1 LGM climate evaluation

3.1.1 Temperature

The LGM-simulated surface ocean is much colder than the HC (3.2°C , see Table 2) with the greatest cooling in the annual averaged SST occurring in the North Pacific, North Atlantic and the Pacific sector of the Southern Ocean (Fig. 1). In comparison to paleo-reconstructions, our simulated LGM cooling was more than 1°C colder than the Waelbroeck et al. (2009) estimates (Table 2), and more comparable to Ballantyne (2005) reconstructed SST cooling over the tropical ocean (30°S – 30°N) of $2.7 \pm 0.5^{\circ}\text{C}$. Our simulation did not produce a large difference in the averaged value of SST cooling between the Atlantic, Pacific and Indian Oceans (less than 0.3°C difference). In contrast, the Waelbroeck et al. (2009) paleo-reconstruction shows more than a 1°C greater cooling in the Atlantic Ocean than the global average (Table 2), while the Ballantyne (2005) reconstructions had regional tropical coolings of 3°C in the Atlantic, 2.5°C in the Indian, and 1°C in the central Pacific Oceans. Perhaps some of the discrepancies between the simulated LGM cooling and paleo-reconstructions reflect the large spatial variability in SST cooling and the limited samples available for the paleo-reconstructions.

As synthesised by Otto-Bliesner et al. (2009), the paleo-reconstructions of SST difference between the HC and LGM based on foraminiferal assemblages display large spatial variability in the tropical oceans. In the eastern tropical Atlantic (east of 25°W), the LGM cooling is in excess of 3°C with several cores suggesting cooling of greater than 5°C (Kucera et al., 2005). In contrast, LGM cooling in the western tropical Atlantic Warm Pool is only 1 to 2°C (Otto-Bliesner et al., 2009). In the tropical Pacific, most cores show LGM cooling of less than 3°C , however several cores suggest cooling of

Earth system model simulations of the LGM

R. J. Matear et al.

Title Page

Abstract

Introduction

Conclusions

References

Tables

Figures



Back

Close

Full Screen / Esc

Printer-friendly Version

Interactive Discussion



sea-ice extent. Sarnthein et al. (2003) LGM reconstructions give a North Atlantic winter maximum sea extent that extends south of Iceland then across to the southern tip of Labrador, which is similar to the simulated LGM maximum sea-ice extent in the North Atlantic (Fig. 2). Both the paleo-reconstructions (Sarnthein et al., 2003) and our LGM simulation show a dramatic retreat of the minimum sea-ice extent to north of Greenland during the summer (Fig. 2).

In the North Pacific, the simulated maximum LGM sea-ice extent went as far south as 45° N, with much greater sea-ice cover in the western Pacific than the eastern Pacific. Consistent with our LGM simulation, paleo-reconstructions suggest that LGM winter sea-ice extent was greater in the western Pacific (Nürnberg and Tiedemann, 2004), with no sea-ice cover at 50° N and 167° E in the Central North Pacific (Jaccard et al., 2005).

During the summer season, the simulated LGM minimum seasonal sea-ice extent rapidly contracts to cover 6.5 and 11.4×10^6 km² in the Southern and Northern Hemispheres, respectively, which is less than 1/3 of the maximum sea-ice extent (Fig. 2). In contrast, the HC simulation had sea ice cover of 1.7 and 5.3×10^6 km² in the Southern and Northern Hemispheres, respectively. The simulated minimum sea-ice extent was much greater in the LGM than the HC with areas in the North Pacific, North Atlantic and Southern Ocean where sea-ice was present throughout the year.

3.1.3 Meridional overturning

Associated with the changes in the surface ocean during the LGM were changes in the meridional overturning circulation. In the LGM simulation, the rate of Antarctic Bottom Water (AABW) formation increased to 15 from 7 Sv in the HC (Fig. 3, minimum in high latitude Southern Hemisphere Global overturning). The LGM simulation also showed greater subduction of Southern Ocean intermediate water than the HC simulation. The simulated LGM North Atlantic Deep Water (NADW) overturning (15 Sv) was similar to the HC simulation (17 Sv), but the cell was shallower in the LGM simulation (maximum

Earth system model simulations of the LGM

R. J. Matear et al.

Title Page

Abstract

Introduction

Conclusions

References

Tables

Figures



Back

Close

Full Screen / Esc

Printer-friendly Version

Interactive Discussion



in the North Atlantic overturning). The LGM simulated meridional overturning showed that the deep water was dominated by water from the Southern Ocean.

The simulated features of meridional overturning in the LGM are supported by the paleo-reconstructions. Paleonutrient tracers indicate that the boundary between NADW and AABW was substantially shallower during the LGM than today (Otto-Bliesner et al., 2007). In our simulations, the NADW cell rises from a maximum depth of 3000 m in the HC to a depth of 1500 m in the LGM. During the LGM, paleonutrient tracers (Yu et al., 1996; McManus et al., 2004) also suggest the North Atlantic Ocean was more stratified, with a shoaling of the NADW cell, and the AABW penetrating much farther into the North Atlantic than at present. The greater contribution of AABW to the deep water of the North Atlantic is also consistent with Atlantic sediment cores that indicate that in the LGM the Atlantic deep waters were much colder and saltier than modern day (Adkins, 2002). The paleo-reconstructions imply that the bottom waters of the LGM were considerably more saline than today and that the deep ocean was more stratified, with the stratification being due to salinity rather than temperature as the bottom temperatures were close to freezing throughout much of the world ocean (Adkins, 2013). The simulated salinity distribution in the LGM was consistent with paleo-reconstructions (Fig. 4). As postulated by Watson and Garabato (2006), the very cold and saline bottom water was the consequence of more production of brines from greater sea-ice formation in the Southern Ocean in the LGM simulation.

Originally, the shoaling of the NADW and greater contribution of AABW to the North Atlantic was interpreted as a significant reduction in NADW formation (McManus et al., 2004; Yu et al., 1996), but more recent paleonutrient tracers suggest that during the LGM, NADW was similar or slightly reduced compared to HC (Otto-Bliesner et al., 2007). This slight reduction and shoaling of the NADW in the LGM was consistent with our simulations.

Earth system model simulations of the LGM

R. J. Matear et al.

Title Page

Abstract

Introduction

Conclusions

References

Tables

Figures



Back

Close

Full Screen / Esc

Printer-friendly Version

Interactive Discussion



**Earth system model
simulations of the
LGM**

R. J. Matear et al.

[Title Page](#)[Abstract](#)[Introduction](#)[Conclusions](#)[References](#)[Tables](#)[Figures](#)[Back](#)[Close](#)[Full Screen / Esc](#)[Printer-friendly Version](#)[Interactive Discussion](#)

rem mineralization of organic matter in the ocean interior. From the apparent oxygen utilization (AOU) of the interior waters and the prescribed ratio of O/P/C of particulate organic matter (POM) used in the model, we computed the amount of phosphate and DIC produced from the remineralization of sinking POM. In the LGM simulation, the remineralized phosphate was much less than the HC simulation, with the total amount of remineralized phosphate being only 40 % of the HC simulation. While the amount of remineralized phosphate declined in the LGM simulation, the phosphate concentrations in the deep water (below 1500 m) were greater than the HC simulation (Fig. 8). The increase in phosphate in the LGM simulation reflects the increased subduction of phosphate-rich AABW which transfers phosphate into the abyss and reduces the phosphate concentrations in the upper ocean (Fig. 8). Paleo cadmium and $\delta^{13}\text{C}$ data from the tropical and North Atlantic show increased nutrient levels in the abyss, but reduced levels above 2000 m during the LGM (Boyle, 1992; Marchitto and Broecker, 2006; Tagliabue et al., 2009). This redistribution of nutrients in the LGM was consistent with our simulated LGM phosphate distribution. The LGM simulation relies on increased AABW subduction to transfer nutrients from the upper ocean into the abyss and elevate DIC, phosphate, alkalinity and oxygen concentrations below 2000 m.

Associated with the transfer of phosphate from the upper ocean into the abyss in the LGM simulation there was a global reduction in the export of POC from the euphotic zone (Table 3). The LGM simulation (Fig. 9) was consistent with paleonutrient data which suggests export production in the Antarctic Zone of the Southern Ocean was lower during the LGM (Jaccard et al., 2005). Similarly, the simulated decline in North Pacific export production (Fig. 9) was consistent with paleonutrient data from the Subarctic Northwest Pacific, which indicates less export production during glacial periods (Jaccard et al., 2005). The simulated reduction of export production in the Subarctic Northwest Pacific and North Atlantic, in regions not covered by sea ice, is caused by reduced phosphate availability (Fig. 10). The equatorial upwelling region of the east Pacific and east Atlantic were two other regions in the LGM simulation where the sur-

sensitivity of the carbon content of the ocean in the LGM to changes in the depth of POC remineralization was much less than suggested by the simulation of Kwon et al. (2009). The reduced sensitivity of carbon storage in our LGM simulation to the depth of POC remineralization reflects the conclusion that the steady-state response is much smaller than the transient response (Schneider et al., 2008).

Finally, the PIC export was set to zero, which was motivated by the strong relationship between calcification and temperature (Lough and Barnes, 2000), i.e. in a cooler ocean less PIC would be produced. With no PIC export, the solubility of CO₂ in the surface water increased and enabled the ocean to store an additional 260 Pg C.

Independently, none of the BGC modifications comes close to increasing the LGM storage of carbon in the ocean above the HC simulation (OLGM-3, 4 and 5, Table 3). By employing all three BGC modifications discussed above in one LGM simulation (OLGM-6), the ocean stored 830 Pg C more than the standard LGM simulation (OLGM-1; Table 4). With all three BGC modifications, the increase in the ocean carbon storage in the LGM simulation was 240 Pg C more than the HC simulation and now comes within the bounds of the combined reduction in atmospheric carbon and terrestrial carbon reported by Ciais et al. (2011) of 520 ± 400 Pg C (Table 4). Combined, the three BGC modifications are sufficient to explain the change in land and atmospheric carbon between the HC and LGM. The consequences of these BGC modifications will next be assessed by looking at how they change the stability of calcium carbonate, export production and dissolved oxygen. However, before exploring these changes we first consider other biogeochemical processes that could account for the additional carbon storage in the ocean.

The carbon stored in the ocean could be increased by increasing alkalinity input from the land due to terrestrial weathering. The 1120 ± 400 Pg C would require an alkalinity increase of 112 ± 40 Pmol Eq (10 % global increase). During the LGM, a drier climate, extensive ice sheets and exposed shelf areas would change terrestrial weathering but such changes are unlikely to have increased alkalinity input from the HC (Brovkin et al., 2007). Therefore, increased alkalinity input into the ocean seems an unlikely explana-

CPD

11, 1093–1142, 2015

Earth system model simulations of the LGM

R. J. Matear et al.

Title Page

Abstract

Introduction

Conclusions

References

Tables

Figures



Back

Close

Full Screen / Esc

Printer-friendly Version

Interactive Discussion



lysocline during the LGM. To have a LGM simulation agree with the paleo observations for south of Tasmania, all three BGC modifications are required (Fig. 13).

3.3.2 Export of particulate organic carbon

In the standard LGM simulation (OLGM-1), the export of POC from the upper ocean generally declines everywhere relative to the HC simulation except on the southern boundary of the eastern equatorial upwelling region of the Pacific (Fig. 14b). The setting of the export of PIC to zero had no impact on POC export, while deepening the POC remineralization increased the transfer of carbon and nutrients into the ocean interior and the POC export was generally reduced everywhere relative to the HC (Fig. 14d). With the POC scaling factor increased, the total POC export was still less than the HC (Table 3), but now the Southern Ocean and small areas of the North Atlantic and Northwest Pacific have increased POC export compared to the HC. The simulation with all three BGC modifications shows a very similar pattern of change as the simulation with just increased POC export (Fig. 14a and c). In this simulation, POC export increased in the Southern Ocean and declined in the subtropics and tropics (Fig. 14a). Such changes to POC export are consistent with paleo-reconstructions of POC differences between the LGM and HC (Sigman et al., 2010). The increase in POC export in the Southern Ocean reduces the phosphate concentrations in the subducted Antarctic Intermediate Waters, which has been shown to be critical to setting the magnitude of the export production outside of the Southern Ocean (Sarmiento et al., 2004).

3.3.3 Dissolved oxygen

The greater subduction of AABW in the LGM dramatically increased the oxygen levels in the ocean and coupled with the decreased remineralization of POC in the ocean there was a large increase in oxygen concentrations in the ocean interior during the standard LGM simulation relative to the HC simulation (55% increase). In the standard LGM simulation, oxygen levels increased in both the intermediate and deep water

Earth system model simulations of the LGM

R. J. Matear et al.

Title Page

Abstract

Introduction

Conclusions

References

Tables

Figures



Back

Close

Full Screen / Esc

Printer-friendly Version

Interactive Discussion



in the volume of anoxic water. In contrast, the deep ocean trace metal records generally suggest a decline in LGM oxygen levels relative to the HC (Jaccard and Galbraith, 2011). Such a decline in LGM oxygen requires oxygen consumption in the deep ocean to increase by an amount that exceeds the temperature-driven increase of oxygen solubility. Such a behaviour is only achieved when all three BGC modifications are used in the LGM simulation.

4 Conclusions

Simulating the earth's climate is a challenging task given the complexity of the climate system, but an ideal way to test our knowledge of the climate system. We have used a 3-D GCM to simulate the climate state during the LGM by changing the orbital parameters and the concentration of greenhouse gases in the atmosphere. Compared with the HC simulation, our simulated LGM showed more than a doubling of the winter sea-ice extent in both hemispheres; a slight reduction and 1000 m shoaling of the NADW overturning; a near doubling in the strength of the AABW overturning; a reduction in temperature and an increase in salinity of the deep water; and an increase in the vertical stratification. A recent review by Adkins (2013) highlighted that the robust changes between the HC and LGM include: a shoaling of the NADW in the Atlantic, increased contribution of AABW to the deep water and a salt-stratified deep ocean (rather than heat-stratified). These changes are reproduced by our simulations, which provides some confidence in using the simulations to investigate what caused the 80–100 ppm reduction in atmospheric CO₂ between the interglacial and glacial periods.

The response of the BGC tracers to the simulated LGM ocean state was a large increase in salinity, oxygen, phosphate, DIC and alkalinity in the deep ocean and an increase in the vertical gradient of these tracers with depth. The increase in the deep water concentrations and in the vertical gradient was due to greater subduction of AABW and not due to increased remineralization of sinking POC. The simulation identified the importance of changes in the subduction of AABW to the BGC tracers. How-

CPD

11, 1093–1142, 2015

Earth system model simulations of the LGM

R. J. Matear et al.

Title Page

Abstract

Introduction

Conclusions

References

Tables

Figures



Back

Close

Full Screen / Esc

Printer-friendly Version

Interactive Discussion



**Earth system model
simulations of the
LGM**

R. J. Matear et al.

[Title Page](#)[Abstract](#)[Introduction](#)[Conclusions](#)[References](#)[Tables](#)[Figures](#)[Back](#)[Close](#)[Full Screen / Esc](#)[Printer-friendly Version](#)[Interactive Discussion](#)

ever, with just these simulated physical changes to the LGM simulation, the storage of carbon in the ocean declined by 600 Pg C from the HC. This reduction in ocean carbon in the LGM simulation reflects the reduced atmospheric CO₂ concentration in the LGM. A subsequent simulation using the simulated LGM climate with an atmospheric CO₂ concentration set to the HC value (280 ppm) shows that the LGM ocean stored 1130 Pg C more than the HC simulation, demonstrating that the simulated LGM ocean was preconditioned to store carbon in the deep ocean. Importantly, this LGM simulation had an aragonite lysocline that was too deep and deep water oxygen concentrations that were too high.

With the simulated LGM climate we explored how to increase the carbon content of the ocean between the LGM and HC and make the simulation more consistent with the aragonite lysocline and deep water oxygen concentrations. The existing paleo data suggest a loss of 520 ± 400 Pg C from the atmosphere and land during the LGM (Ciais et al., 2011). To increase the carbon stored in the LGM ocean we considered three plausible modifications to the biogeochemical processes in the ocean: (1) increased POC export due to increased atmospheric iron deposition, (2) increased depth of POC remineralization due to cooler interior water, (3) no PIC export due to colder surface water. Each process increased the ocean carbon storage but separately they could not account for the total decline in atmosphere and land carbon. However, when combined in one simulation the ocean carbon storage was 240 Pg C greater than the simulated HC ocean and now within the bounds of the required increased carbon storage (520 ± 400 Pg C Ciais et al., 2011). The simulated differences between the HC and LGM with the three BGC modifications was also more consistent with paleo-reconstructions than the simulation without the BGC modifications. These include the presence of less anoxic water, a less than 1000 m deepening of the lysocline in the North Pacific and Southern Ocean, the reduction in POC export, the increase in nutrient-limited conditions in the LGM, and deep water oxygen levels that did decline in the Southern Ocean. Further, the surface Ω values were nearly equivalent to the HC values.

Earth system model simulations of the LGM

R. J. Matear et al.

Title Page

Abstract

Introduction

Conclusions

References

Tables

Figures



Back

Close

Full Screen / Esc

Printer-friendly Version

Interactive Discussion



Our GCM simulations produced a plausible LGM state, which provides some confidence in our ability to model the complex climate system. With the inclusion of the BGC in the simulation we generated new information to assess the simulated climate and pursue the link between climate and the global carbon cycle. While the simulations have shown the need to modify ocean BGC processes to increase the carbon storage in the ocean we now need to better constrain these modifications. A key future effort will be to better quantify the BGC process that could increase the carbon stored in the ocean in a manner that is consistent with 3-D paleo-reconstructions.

Appendix: Ocean biogeochemical model equations

The ocean BGC module used in this study is the same one as used by Matear and Lenton (2014) and is based on an earlier model by Matear and Hirst (2003). For a complete description of the model refer to the Appendix in Matear and Lenton (2014). Here we provide the basic description of the model to enable the reader to follow the BGC modifications performed in this study.

The ocean BGC module links the biological export of particulate organic carbon from the euphotic zone (POC) to phosphate, light, temperature and mixed layer parameterizations. The BGC model fixes the ratio of POC and particulate inorganic carbon (PIC) export from the euphotic zone (50 m) and prescribes the depth-dependent remineralization equations for POC and PIC. The key equations for these processes are summarized below.

In the euphotic zone, which is set to be the surface layer of the model (upper 50 m), biological formation of particulate organic and inorganic matter occurs. For particulate organic matter, the production of particulate organic phosphorus (POP) was defined by the following equations:

$$V_{\max} = 0.6(1.066)^T \quad (\text{A1})$$

$$F(I) = \left[1 - e^{R(I)} \right] \quad (\text{A2})$$

$$R(I) = \frac{I(x, t)\alpha\text{PAR}}{V_{\max}} \quad (\text{A3})$$

$$J(P) = S_{\text{pp}}V_{\max}\min\left(\frac{P}{P + P_k}, F(I)\right)\Delta z \quad (\text{A4})$$

V_{\max} is the maximum growth rate in day^{-1} , which is a function of the surface layer temperature (T , [$^{\circ}\text{C}$]). $F(I)$ is the productivity vs. irradiance equation used to describe phytoplankton growth, which is given as a unitless value and provides a measure of light-limited growth. $R(I)$ is a unitless function of the light availability for growth, which comes from the incident short wave radiation (I in W m^{-2}) scaled by photosynthetic active radiation PAR (unitless factor), and the initial slope (α) of the productivity vs. radiance curve for phytoplankton growth [$\text{day}^{-1} (\text{W m}^{-2})^{-1}$]. $J(P)$ gives the production of POP in $\text{mmol m}^{-2} \text{P day}^{-1}$, which is function of a tuneable parameter (S_{pp}) in $\text{mmol m}^{-3} \text{P}$, the thickness of the surface layer (Δz) in meters and the growth limitation function. The growth limitation function compares nutrient- and light-limited growth and uses the minimum value. The nutrient-limited term is based on the P of the surface layer and half-saturation uptake (P_k) value for phosphate utilization.

A constant value was used to link the POP production to the organic carbon, oxygen and alkalinity sink as follows:

$$J(C) = 106J(P) \quad (\text{A5})$$

$$J(O) = -136J(P) \quad (\text{A6})$$

$$J(A) = -16J(P) \quad (\text{A7})$$

The PIC export (K) in the model was linked to POC by using a fixed rain ratio of 8% to give the following sinks of carbon and alkalinity:

$$K(C) = 0.08 \times 106 J(P) \quad (\text{A8})$$

$$K(A) = 0.08 \times 2 \times 106 J(P) \quad (\text{A9})$$

Earth system model simulations of the LGM

R. J. Matear et al.

Title Page

Abstract

Introduction

Conclusions

References

Tables

Figures



Back

Close

Full Screen / Esc

Printer-friendly Version

Interactive Discussion



The POC and PIC produced in the euphotic zone was instantaneously remineralized in the ocean interior over where it was produced according to the following equation:

$$r\text{POC}(z) = \text{POC} \times \left(\frac{z}{100\text{ m}} \right)^{-0.9} \quad (\text{A10})$$

$$r\text{PIC}(z) = \text{PIC} \times \exp [z/3500\text{ m}] \quad (\text{A11})$$

where POC and PIC denote the exports from the euphotic zone and z is depth in meters. No remineralization occurs above 100 m.

Acknowledgements. Funding for this work was provided by the Australian Climate Change Science Program and CSIRO Wealth from Ocean Flagship. This work was also supported by an award under the Merit Allocation Scheme on the NCI National Facility at the Australian National University. The authors wish to acknowledge the use of the Ferret program for the analysis and graphics presented in the paper (<http://ferret.pmel.noaa.gov/Ferret/>).

References

- Abbey, E., Webster, J. M., and Beaman, R. J.: Geomorphology of submerged reefs on the shelf edge of the Great Barrier Reef: the influence of oscillating Pleistocene sea-levels, *Mar. Geol.*, 288, 61–78, 2011. 1109
- Adkins, J. F.: The salinity, temperature, and $\delta^{18}\text{O}$ of the glacial deep ocean, *Science*, 298, 1769–1773, 2002. 1101
- Adkins, J. F.: The role of deep ocean circulation in setting glacial climates, *Paleoceanography*, 28, 539–561, 2013. 1101, 1112
- Anderson, D. and Archer, D. E.: Glacial-interglacial stability of ocean pH inferred from foraminifer dissolution rates, *Nature*, 416, 70–73, 2002. 1109
- Archer, D., Winguth, A., Lea, D., and Mahowald, N.: What caused the glacial/interglacial atmospheric $p\text{CO}_2$ cycles?, *Rev. Geophys.*, 38, 159–189, 2000. 1095
- Ballantyne, A. P.: Meta-analysis of tropical surface temperatures during the Last Glacial Maximum, *Geophys. Res. Lett.*, 32, L05712, doi:10.1029/2004GL021217, 2005. 1098
- Boyle, E. A.: Cadmium and $\delta^{13}\text{C}$ paleochemical ocean distributions during the stage 2 glacial maximum, *Annu. Rev. Earth Pl. Sc.*, 20, 245–287, 1992. 1103

Title Page

Abstract

Introduction

Conclusions

References

Tables

Figures



Back

Close

Full Screen / Esc

Printer-friendly Version

Interactive Discussion



**Earth system model
simulations of the
LGM**

R. J. Matear et al.

[Title Page](#)[Abstract](#)[Introduction](#)[Conclusions](#)[References](#)[Tables](#)[Figures](#)[Back](#)[Close](#)[Full Screen / Esc](#)[Printer-friendly Version](#)[Interactive Discussion](#)

- Broecker, W. S. and Henderson, G. M.: The sequence of events surrounding Termination II and their implications for the cause of glacial-interglacial CO₂ changes, *Paleoceanography*, 13, 352–364, 1998. 1095
- Brovkin, V., Ganopolski, A., Archer, D. E., and Rahmstorf, S.: Lowering of glacial atmospheric CO₂ in response to changes in oceanic circulation and marine biogeochemistry, *Paleoceanography*, 22, PA4202, doi:10.1029/2006PA001380, 2007. 1095, 1106
- Catubig, N., Archer, D. E., Francois, R., deMenocal, P., Howard, W., and Yu, E.: Global deep-sea burial rate of calcium carbonate during the last glacial maximum, *Paleoceanography*, 13, 298–310, 1998. 1109
- Chen, M., Huang, C., Pflaumann, U., Waelbroeck, C., and Kucera, M.: Estimating glacial western Pacific sea-surface temperature: methodological overview and data compilation of surface sediment planktic foraminifer faunas, *Quaternary Sci. Rev.*, 24, 1049–1062, 2005. 1099
- Ciais, P., Tagliabue, A., Cuntz, M., Bopp, L., Scholze, M., Hoffmann, G., Lourantou, A., Harrison, S. P., Prentice, I. C., Kelley, D. I., Koven, C., and Piao, S. L.: Large inert carbon pool in the terrestrial biosphere during the Last Glacial Maximum, *Nat. Geosci.*, 5, 74–79, 2011. 1106, 1107, 1113, 1125
- Comiso, J. C.: Large-scale Characteristics and Variability of the Global Sea Ice Cover, in: *Sea Ice: An Introduction to its Physics, Chemistry, Biology and Geology*, edited by: Thomas, D. N. and Dieckmann, G. S., Blackwell Science Ltd, Oxford, UK, doi:10.1002/9780470757161.ch4, 2003. 1099
- Falkowski, P., Scholes, R., Boyle, E., Canadell, J., Canfield, D., Elser, J., Gruber, N., Hibbard, K., Hogberg, P., Linder, S., Mackenzie, F., Moore, B., Pedersen, T., Rosenthal, Y., Seitzinger, S., Smetacek, V., and Steffen, W.: The global carbon cycle: a test of our knowledge of earth as a system, *Science*, 290, 291–296, 2000. 1095
- Galbraith, E., Kienast, M., Pedersen, T., and Calvert, S.: Glacial-interglacial modulation of the marine nitrogen cycle by high-latitude O₂ supply to the global thermocline, *Paleoceanography*, 19, PA4007, doi:10.1029/2003PA001000, 2004. 1111
- Garcia, H., Locarnini, R., and Boyer, T.: World ocean atlas 2005, Volume 3: Dissolved oxygen, apparent oxygen utilization, in: *NOAA Atlas NESDIS 63*, edited by: Levitus, S., U.S. Government Printing Office, Washington, D.C., 342 pp., 2006a. 1130, 1135, 1140
- Garcia, H., Locarnini, R., Boyer, T., and Antonov, J.: World ocean atlas 2005, Volume 4: Nutrients (phosphate, nitrate, silicate), in: *NOAA Atlas NESDIS 63*, edited by: Levitus, S., U.S. Government Printing Office, Washington, D.C., 396 pp., 2006b. 1133

Earth system model simulations of the LGM

R. J. Matear et al.

[Title Page](#)

[Abstract](#)

[Introduction](#)

[Conclusions](#)

[References](#)

[Tables](#)

[Figures](#)



[Back](#)

[Close](#)

[Full Screen / Esc](#)

[Printer-friendly Version](#)

[Interactive Discussion](#)



- Gersonde, R., Crosta, X., Abelmann, A., and Armand, L.: Sea-surface temperature and sea lee distribution of the Southern Ocean at the EPILOG Last Glacial Maximum - A circum-Antarctic view based on siliceous microfossil records, *Quaternary Sci. Rev.*, 24, 869–896, 2005. 1099
- Hoegh-Guldberg, O., Mumby, P. J., Hooten, A. J., Steneck, R. S., Greenfield, P., Gomez, E., Harvell, C. D., Sale, P. F., Edwards, A. J., Caldeira, K., Knowlton, N., Eakin, C. M., Iglesias-Prieto, R., Muthiga, N., Bradbury, R. H., Dubi, A., and Hatziolos, M. E.: Coral reefs under rapid climate change and ocean acidification, *Science*, 318, 1737–1742, 2007. 1108
- Jaccard, S. L. and Galbraith, E. D.: Large climate-driven changes of oceanic oxygen concentrations during the last deglaciation, *Nat. Geosci.*, 5, 151–156, 2011. 1111, 1112
- Jaccard, S., Haug, G., Sigman, D., Pedersen, T., Thierstein, H., and Rohl, U.: Glacial/interglacial changes in subarctic North Pacific stratification, *Science*, 308, 1003–1006, 2005. 1100, 1103
- Key, R. M., Kozyr, A., Sabine, C. L., Lee, K., Wanninkhof, R., Bullister, J. L., Feely, R. A., Millero, F. J., Mordy, C., and Peng, T. H.: A global ocean carbon climatology: Results from Global Data Analysis Project (GLODAP), *Global Biogeochem. Cy.*, 18, GB4031, doi:10.1029/2004GB002247, 2004. 1131, 1132, 1136, 1137
- Kucera, M., Weinelt, M., Kiefer, T., Pflaumann, U., Hayes, A., Weinelt, M., Chen, M., Mix, A., Barrows, T., Cortijo, E., Duprat, J., Juggins, S., and Waelbroeck, C.: Reconstruction of sea-surface temperatures from assemblages of planktonic foraminifera: multi-technique approach based on geographically constrained calibration data sets and its application to glacial Atlantic and Pacific Oceans, *Quaternary Sci. Rev.*, 24, 951–998, 2005. 1098, 1099
- Kwon, E. Y., Primeau, F., and Sarmiento, J. L.: The impact of remineralization depth on the air–sea carbon balance, *Nat. Geosci.*, 2, 630–635, 2009. 1106
- Langdon, C., Takahashi, T., Sweeney, C., Chipman, D., Goddard, J., Marubini, F., Aceves, H., Barnett, H., and Atkinson, M. J.: Effect of calcium carbonate saturation state on the calcification rate of an experimental coral reef, *Global Biogeochem. Cy.*, 14, 639–654, 2000. 1108
- Levitus, S.: *World Ocean Database*, vol. 13, US Department of Commerce, National Oceanic and Atmosphere Agency, 2001. 1126, 1129
- Lough, J. and Barnes, D.: Environmental controls on growth of the massive coral *Porites*, *J. Exp. Mar. Biol. Ecol.*, 245, 225–243, 2000. 1106
- Marchitto, T. M. and Broecker, W. S.: Deep water mass geometry in the glacial Atlantic Ocean: a review of constraints from the paleonutrient proxy Cd/Ca, *Geochem. Geophys. Geosy.*, 7, Q12003, doi:10.1029/2006GC001323, 2006. 1103

Earth system model simulations of the LGM

R. J. Matear et al.

Title Page

Abstract

Introduction

Conclusions

References

Tables

Figures



Back

Close

Full Screen / Esc

Printer-friendly Version

Interactive Discussion



- Martin, J. H.: Glacial-interglacial CO₂ change: the iron hypothesis, *Paleocoenography*, 5, 1–13, 1990. 1095, 1105
- Matear, R. J. and Hirst, A. C.: Long term changes in dissolved oxygen concentrations in the ocean caused by protracted global warming, *Global Biogeochem. Cy.*, 17, 1125, doi:10.1029/2002GB001997, 2003. 1114
- Matear, R. J. and Lenton, A.: Quantifying the impact of ocean acidification on our future climate, *Biogeosciences*, 11, 3965–3983, doi:10.5194/bg-11-3965-2014, 2014. 1096, 1114
- McManus, J. F., Francois, R., Gherardi, J. M., Keigwin, L. D., and Brown-Leger, S.: Collapse and rapid resumption of Atlantic meridional circulation linked to deglacial climate changes, *Nature*, 428, 834–837, 2004. 1101
- Meissner, K., Galbraith, E., and Völker, C.: Denitrification under glacial and interglacial conditions: a physical approach, *Paleoceanography*, 20, PA3001, doi:10.1029/2004PA001083, 2005. 1111
- Nameroff, T., Calvert, S., and Murray, J.: Glacial-interglacial variability in the eastern tropical North Pacific oxygen minimum zone recorded by redox-sensitive trace metals, *Paleoceanography*, 19, PA1010, doi:10.1029/2003, 2004. 1111
- Nürnberg, D. and Tiedemann, R.: Environmental change in the Sea of Okhotsk during the last 1.1 million years, *Paleoceanography*, 19, PA4011, doi:10.1029/2004PA001023, 2004. 1100
- Otto-Bliesner, B. L., Hewitt, C. D., Marchitto, T. M., Brady, E., Abe-Ouchi, A., Crucifix, M., Murakami, S., and Weber, S. L.: Last Glacial Maximum ocean thermohaline circulation: PMIP2 model intercomparisons and data constraints, *Geophys. Res. Lett.*, 34, L12706, doi:10.1029/2007GL029475, 2007. 1101, 1104
- Otto-Bliesner, B. L., Schneider, R., Brady, E. C., Kucera, M., Abe-Ouchi, A., Bard, E., Braconnot, P., Crucifix, M., Hewitt, C. D., Kageyama, M., Marti, O., Paul, A., Rosell-Melé, A., Waelbroeck, C., Weber, S. L., Weinelt, M., and Yu, Y.: A comparison of PMIP2 model simulations and the MARGO proxy reconstruction for tropical sea surface temperatures at last glacial maximum, *Clim. Dynam.*, 32, 799–815, 2009. 1098, 1099
- Peacock, S., Lane, E., and Restrepo, J. M.: A possible sequence of events for the generalized glacial-interglacial cycle, *Global Biogeochem. Cy.*, 20, GB2010, doi:10.1029/2005GB002448, 2006. 1095
- Phipps, S. J., Rotstayn, L. D., Gordon, H. B., Roberts, J. L., Hirst, A. C., and Budd, W. F.: The CSIRO Mk3L climate system model version 1.0 – Part 1: Description and evaluation, *Geosci. Model Dev.*, 4, 483–509, doi:10.5194/gmd-4-483-2011, 2011. 1096

Earth system model simulations of the LGM

R. J. Matear et al.

Title Page

Abstract

Introduction

Conclusions

References

Tables

Figures



Back

Close

Full Screen / Esc

Printer-friendly Version

Interactive Discussion



- Phipps, S. J., Rotstayn, L. D., Gordon, H. B., Roberts, J. L., Hirst, A. C., and Budd, W. F.: The CSIRO Mk3L climate system model version 1.0 – Part 2: Response to external forcings, *Geosci. Model Dev.*, 5, 649–682, doi:10.5194/gmd-5-649-2012, 2012. 1096
- Rivkin, R. B.: Biogenic carbon cycling in the upper ocean: effects of microbial respiration, *Science*, 291, 2398–2400, 2001. 1105
- Sarmiento, J. L., Gruber, N., Brzezinski, M. A., and Dunne, J. P.: High-latitude controls of thermocline nutrients and low latitude biological productivity, *Nature*, 427, 56–60, 2004. 1110
- Sarnthein, M., Pflaumann, U., and Weinelt, M.: Past extent of sea ice in the northern North Atlantic inferred from foraminiferal paleotemperature estimates, *Paleoceanography*, 18, 1047, doi:10.1029/2002PA000771, 2003. 1100
- Schneider, B., Bopp, L., and Gehlen, M.: Assessing the sensitivity of modeled air-sea CO₂ exchange to the remineralization depth of particulate organic and inorganic carbon, *Global Biogeochem. Cy.*, 22, GB3021, doi:10.1029/2007GB003100, 2008. 1106
- Sigman, D. M., Hain, M. P., and Haug, G. H.: The polar ocean and glacial cycles in atmospheric CO₂ concentration, *Nature*, 466, 47–55, 2010. 1094, 1095, 1110
- Stephens, B. B. and Keeling, R. F.: The influence of Antarctic sea ice on glacial-interglacial CO₂ variations, *Nature*, 404, 171–174, 2000. 1095
- Tagliabue, A., Bopp, L., Roche, D. M., Bouttes, N., Dutay, J.-C., Alkama, R., Kageyama, M., Michel, E., and Paillard, D.: Quantifying the roles of ocean circulation and biogeochemistry in governing ocean carbon-13 and atmospheric carbon dioxide at the last glacial maximum, *Clim. Past*, 5, 695–706, doi:10.5194/cp-5-695-2009, 2009. 1095, 1103, 1105, 1107
- Tamburini, F. and Föllmi, K. B.: Phosphorus burial in the ocean over glacial-interglacial time scales, *Biogeosciences*, 6, 501–513, doi:10.5194/bg-6-501-2009, 2009. 1107
- Thiagarajan, N.: Movement of deep-sea coral populations on climatic timescales, *P. Natl. Acad. Sci. USA*, 28, 227–236, 2012. 1109
- Toggweiler, J. and Russell, J.: Midlatitude westerlies, atmospheric CO₂, and climate change during the ice ages, *Paleoceanography*, PA2005, doi:10.1029/2005PA001154, 2006. 1095
- Waelbroeck, C., Paul, A., Kucera, M., Rosell-Melé, A., Weinelt, M., Schneider, R., Mix, A. C., Abelmann, A., Armand, L., Bard, E., Barker, S., Barrows, T. T., Benway, H., Cacho, I., Chen, M. T., Cortijo, E., Crosta, X., de Vernal, A., Dokken, T., Duprat, J., Elderfield, H., Eynaud, F., Gersonde, R., Hayes, A., Henry, M., Hillaire-Marcel, C., Huang, C. C., Jansen, E., Juggins, S., Kallel, N., Kiefer, T., Kienast, M., Labeyrie, L., Leclaire, H., Londeix, L., Mangin, S., Matthiessen, J., Marret, F., Meland, M., Morey, A. E., Mulitza, S., Pflaumann, U.,

Pisias, N. G., Radi, T., Rochon, A., Rohling, E. J., Sbaiffi, L., Schaefer-Neth, C., Solignac, S., Spero, H., Tachikawa, K., Turon, J. L., and Members, M. P.: Constraints on the magnitude and patterns of ocean cooling at the Last Glacial Maximum, *Nat. Geosci.*, 2, 127–132, 2009. 1098, 1123

- 5 Watson, A. and Garabato, A.: The role of Southern Ocean mixing and upwelling in glacial-interglacial atmospheric CO₂ change, *Tellus B*, 58, 73–87, 2006. 1101
- Yokoyama, Y., Webster, J. M., Cotterill, C., Braga, J. C., Jovane, L., Mills, H., Morgan, S., Suzuki, A., and the IODP Expedition 325 Scientists: IODP Expedition 325: The Great Barrier Reefs Reveal Past Sea-Level, Climate and Environmental Changes Since the Last Ice Age, Scientific Drilling, 2011. 1109
- 10 Yu, E., Francois, R., and Bacon, M.: Similar rates of modern and last-glacial ocean thermohaline circulation inferred from radiochemical data, *Nature*, 379, 689–694, 1996. 1101

CPD

11, 1093–1142, 2015

Earth system model simulations of the LGM

R. J. Matear et al.

Title Page

Abstract

Introduction

Conclusions

References

Tables

Figures



Back

Close

Full Screen / Esc

Printer-friendly Version

Interactive Discussion



Earth system model simulations of the LGM

R. J. Matear et al.

Table 3. Global ocean averaged diagnostics from the model simulations described in Table 1. The subscript organic refers to the inventory due to the remineralization computed from the apparent oxygen utilization. POC and PIC refer to the annual export of particulate organic and inorganic carbon from the upper 50 m, respectively. The tracer columns refer to global ocean inventory or global ocean average values. Global inventory of phosphate was 2.68 Pmol in all simulations.

Model	Atmospheric CO ₂ (ppm)	POC (PgC y ⁻¹)	PIC (PgC y ⁻¹)	Carbon (PgC)	Δ Carbon ¹ (PgC)	C _{organic} (PgC)	Oxygen (Pmol)	P _{organic} (Pmol)	Alkalinity (Pmol Eq)	Salinity	Temperature (°C)
OHC-1	280.0	8.01	0.64	33 974.0	0.0	1650.0	232.0	1.30	3003.0	34.505	3.992
OHC-2	185.0	8.01	0.64	32 206.0	-1560	1650.0	232.0	1.30	3001.0	34.505	3.992
OLGM-1	185.0	4.48	0.36	33 370.0	-604.0	667.0	360.0	0.52	3054.0	35.099	1.649
OLGM-2	280.0	4.48	0.36	33 145.0	1127.0	667.0	360.0	0.52	3055.0	35.099	1.649
OLGM-3	185.0	4.48	0.00	33 407.0	-342.0	667.0	360.0	0.52	3055.0	35.099	1.649
OLGM-4	185.0	5.92	0.47	33 333.0	-416.0	772.0	348.0	0.61	3055.0	35.099	1.649
OLGM-5	185.0	3.25	0.26	33 295.0	-454.0	721.0	354.0	0.57	3054.0	35.099	1.649
OLGM-6	185.0	4.82	0.00	34 213.0	239.0	1004.0	323.0	0.79	3055.0	35.099	1.649

¹ Change in the ocean inventory of carbon relative to the OHC-1 simulation with atmospheric CO₂ at 280 ppm.

[Title Page](#)
[Abstract](#)
[Introduction](#)
[Conclusions](#)
[References](#)
[Tables](#)
[Figures](#)

[Back](#)
[Close](#)
[Full Screen / Esc](#)
[Printer-friendly Version](#)
[Interactive Discussion](#)


Earth system model simulations of the LGM

R. J. Matear et al.

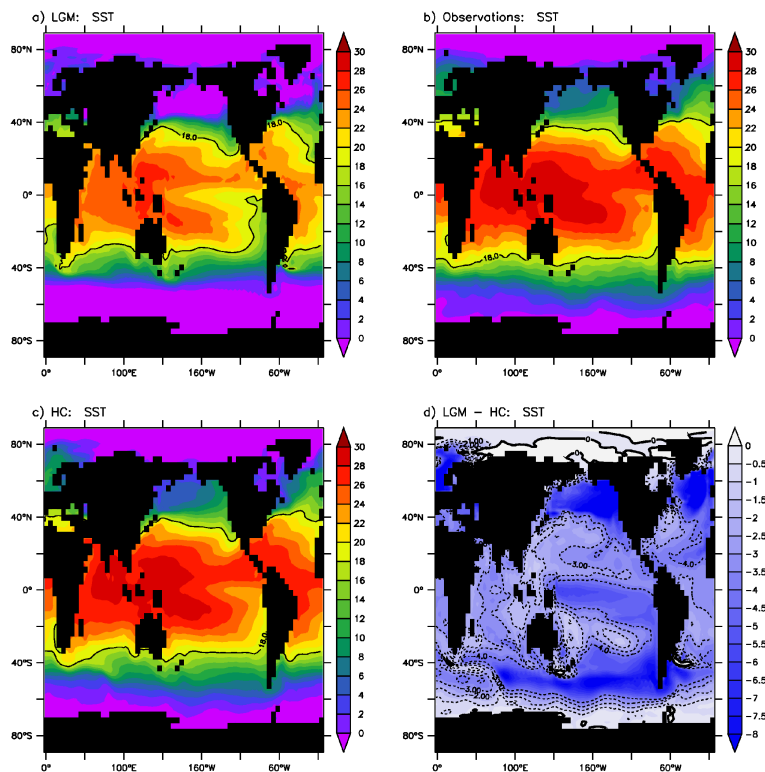


Figure 1. Annual sea surface temperature (SST) for (a) the LGM simulation (OLGM-1), (b) the observations from Levitus (2001), (c) the HC simulation (OHC-1) and (d) the simulated LGM–HC difference (OLGM-1 – OHC-1). In panels (a–c) the black line denotes the 18 °C isotherm.

Title Page

Abstract

Introduction

Conclusions

References

Tables

Figures



Back

Close

Full Screen / Esc

Printer-friendly Version

Interactive Discussion



Earth system model
simulations of the
LGM

R. J. Matear et al.

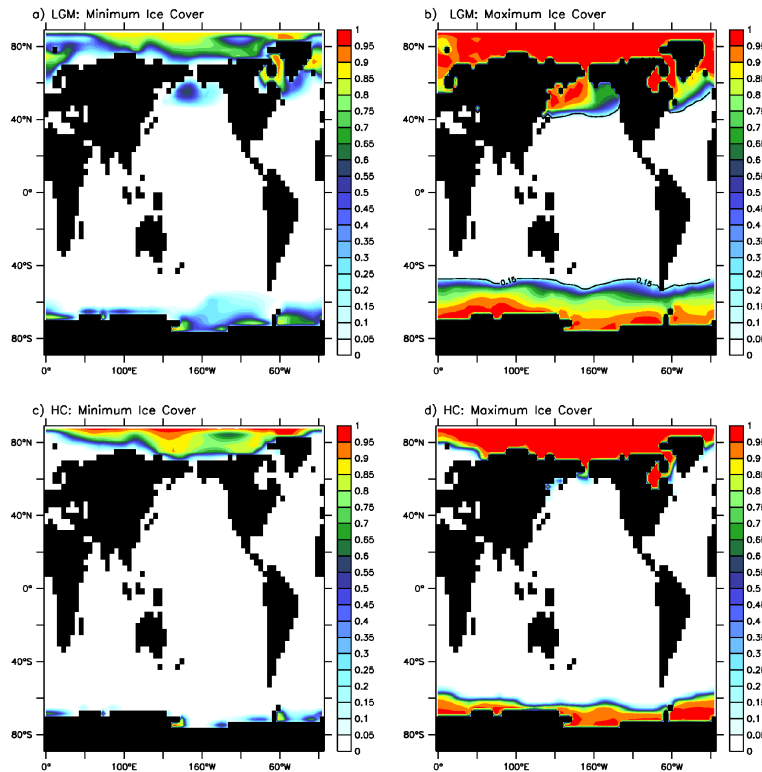


Figure 2. Fraction of sea-ice cover for the annual monthly minimum (left) and annual monthly maximum (right) from the LGM (top) and the HC (bottom) simulations.

[Title Page](#)[Abstract](#)[Introduction](#)[Conclusions](#)[References](#)[Tables](#)[Figures](#)[Back](#)[Close](#)[Full Screen / Esc](#)[Printer-friendly Version](#)[Interactive Discussion](#)

Earth system model simulations of the LGM

R. J. Matear et al.

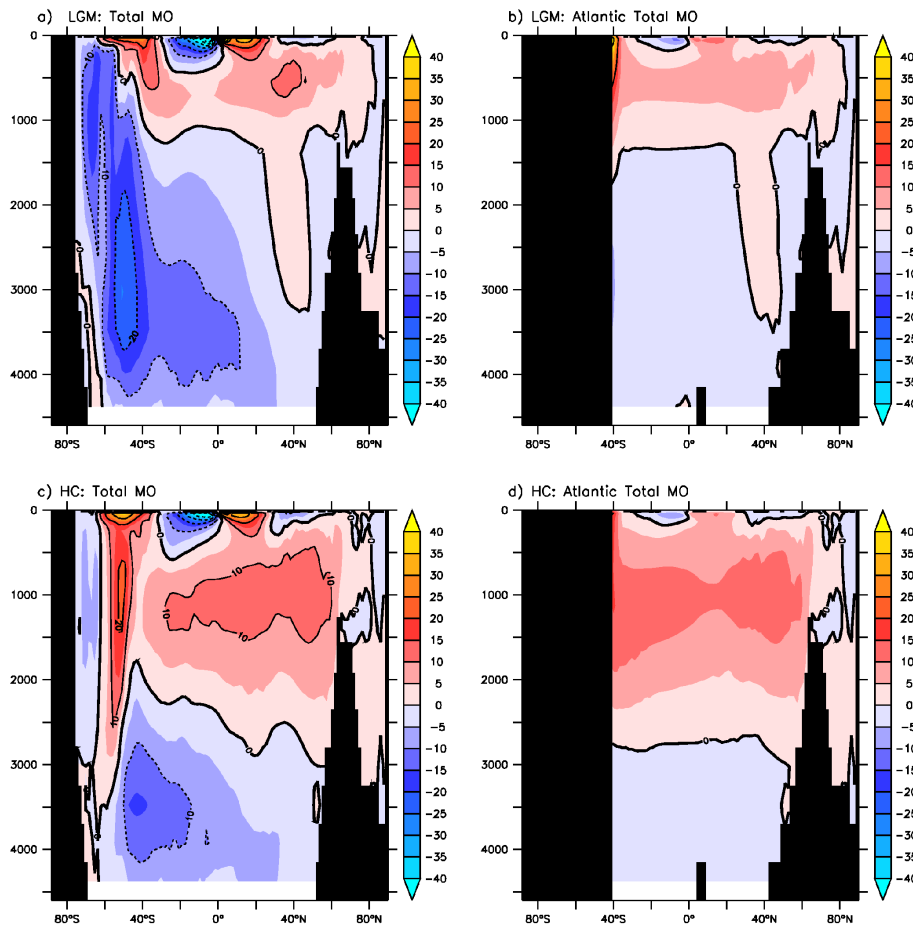


Figure 3. Global meridional overturning (left) and Atlantic meridional overturning (right) in Sv for the LGM (top) and HC (bottom) simulations.

Earth system model simulations of the LGM

R. J. Matear et al.

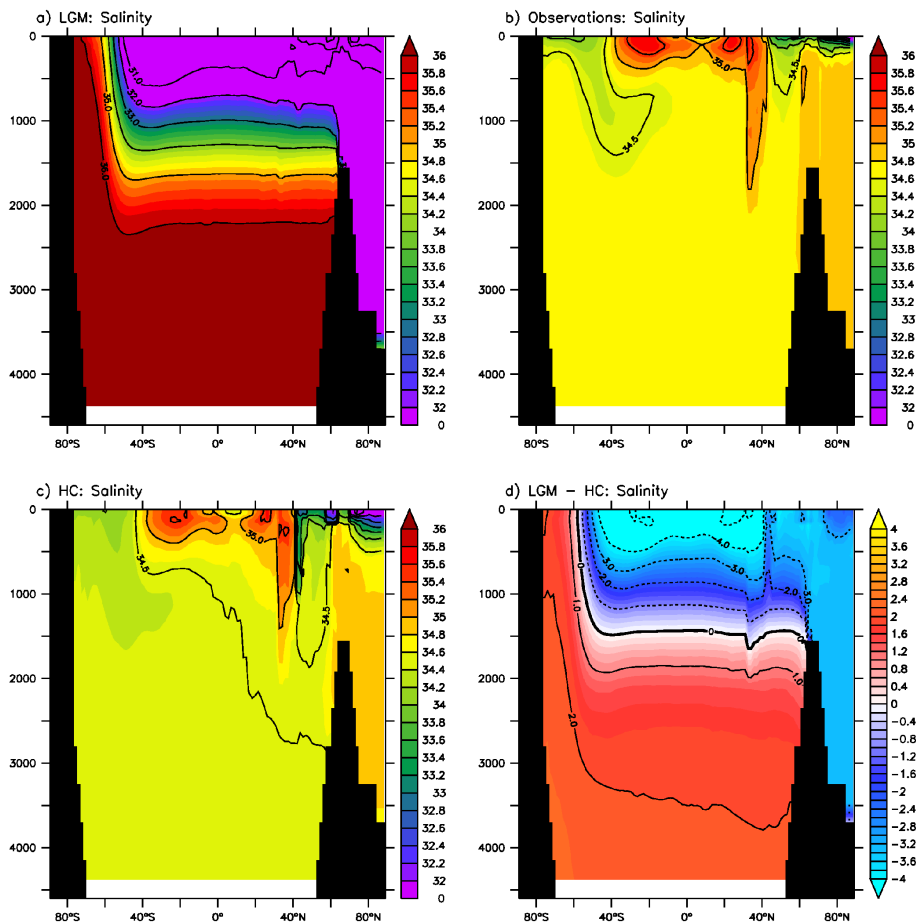


Figure 4. Zonal average salinity for **(a)** the LGM simulation (OLGM-1), **(b)** the observations from Levitus (2001), **(c)** the HC simulation (OHC-1) and **(d)** the simulated LGM–HC difference (OLGM-1 – OHC-1).

[Title Page](#)
[Abstract](#)
[Introduction](#)
[Conclusions](#)
[References](#)
[Tables](#)
[Figures](#)

[Back](#)
[Close](#)
[Full Screen / Esc](#)
[Printer-friendly Version](#)
[Interactive Discussion](#)

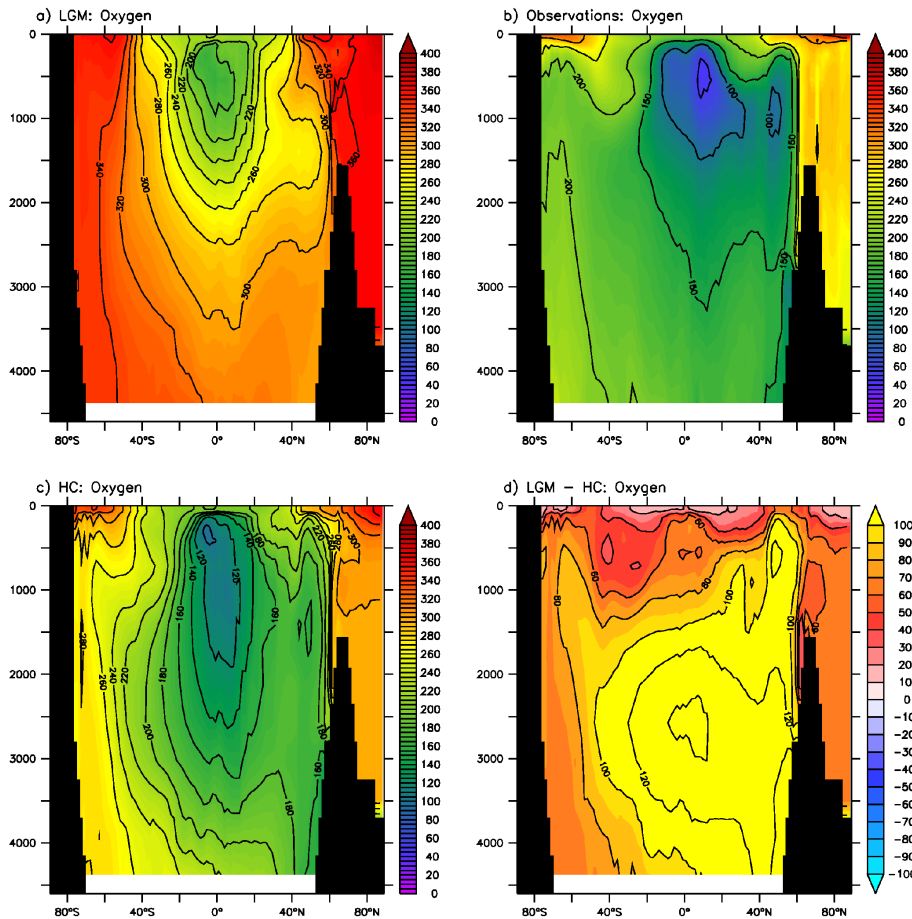



Figure 5. Zonal average dissolved oxygen (mmol m^{-3}) for **(a)** the LGM simulation (OLGM-1), **(b)** the observations from Garcia et al. (2006a), **(c)** the HC simulation (OHC-1) and **(d)** the simulated LGM–HC difference (OLGM-1 – OHC-1).

Earth system model
simulations of the
LGM

R. J. Matear et al.

Title Page

Abstract

Introduction

Conclusions

References

Tables

Figures



Back

Close

Full Screen / Esc

Printer-friendly Version

Interactive Discussion

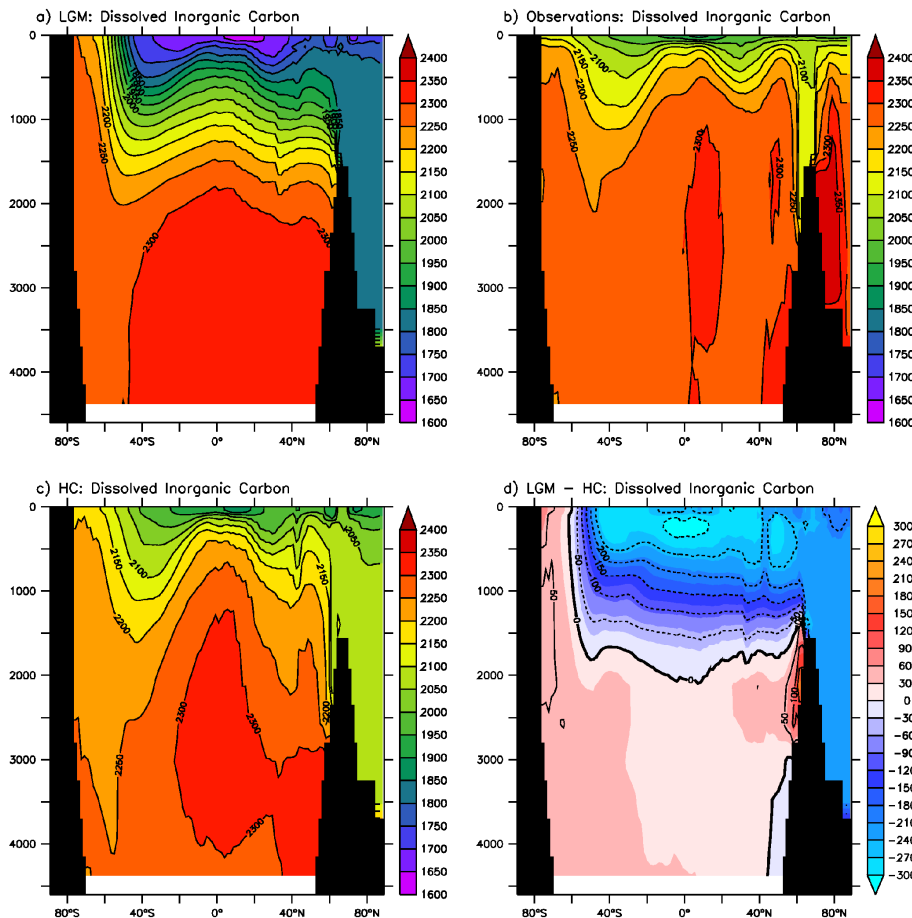


Figure 6. Zonal average dissolved inorganic carbon (mmol m^{-3}) for **(a)** the LGM simulation (OLGM-1), **(b)** the observations from Key et al. (2004), **(c)** the HC simulation (OHC-1) and **(d)** the simulated LGM–HC difference (OLGM-1 – OHC-1).

Earth system model simulations of the LGM

R. J. Matear et al.

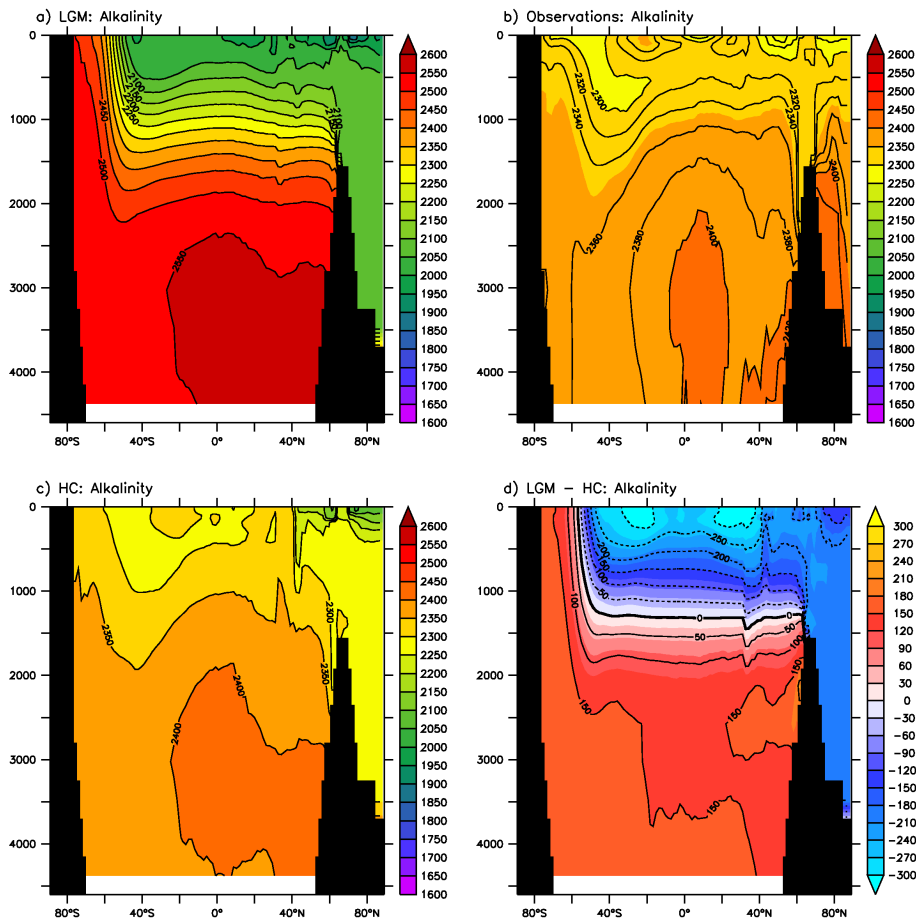


Figure 7. Zonal average alkalinity ($\mu\text{mol Eq m}^{-3}$) for **(a)** the LGM simulation (OLGM-1), **(b)** the observations from Key et al. (2004), **(c)** the HC simulation (OHC-1) and **(d)** the simulated LGM–HC difference (OLGM-1 – OHC-1).

[Title Page](#)
[Abstract](#)
[Introduction](#)
[Conclusions](#)
[References](#)
[Tables](#)
[Figures](#)

[Back](#)
[Close](#)
[Full Screen / Esc](#)
[Printer-friendly Version](#)
[Interactive Discussion](#)

Earth system model
simulations of the
LGM

R. J. Matear et al.

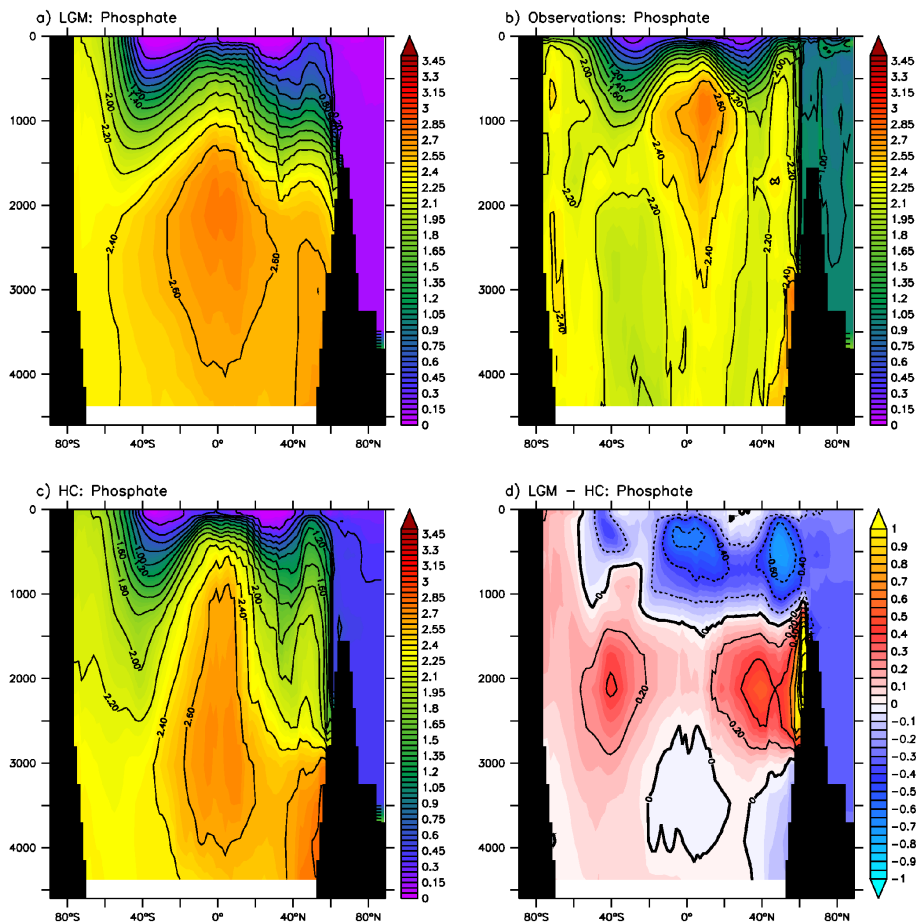


Figure 8. Zonal average phosphate concentration (mmol m^{-3}) for (a) the LGM simulation (OLGM-1), (b) the observations from Garcia et al. (2006b), (c) the HC simulation (OHC-1) and (d) the simulated LGM–HC difference (OLGM-1 – OHC-1).

Earth system model simulations of the LGM

R. J. Matear et al.

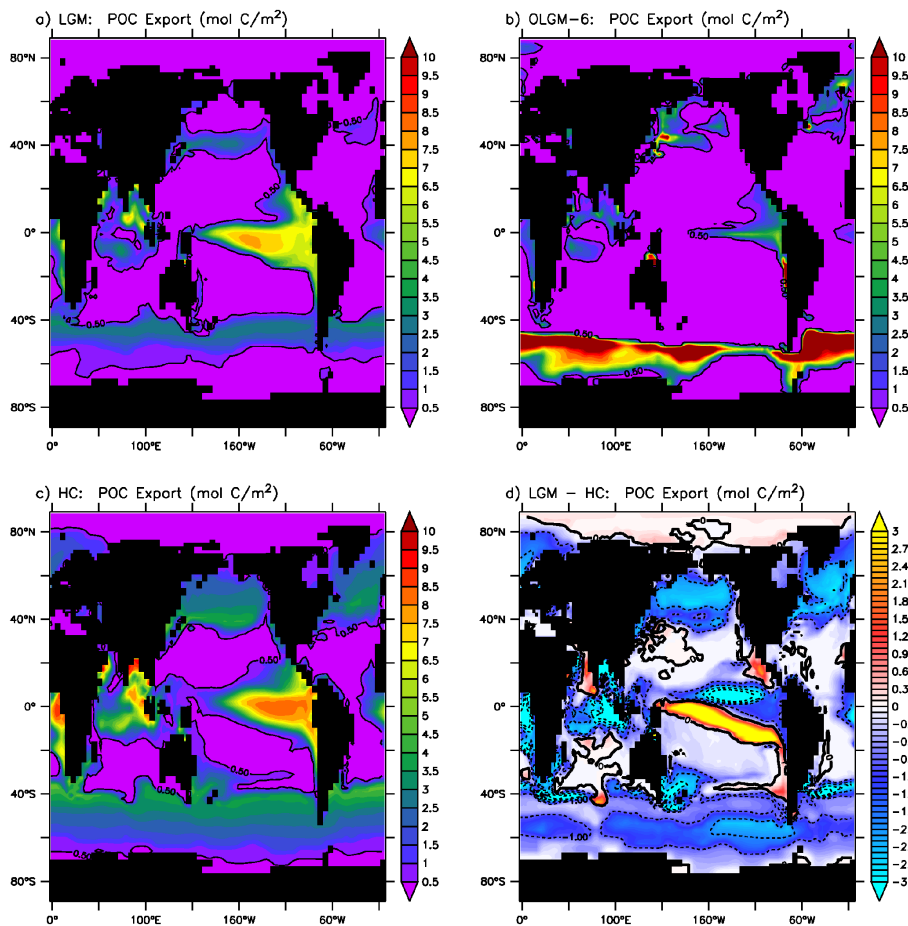


Figure 9. Annual export of particulate organic carbon from the upper 50 m ($\text{g C m}^{-2} \text{y}^{-1}$) for (a) the LGM simulation (OLGM-1), (b) OLGM-6 simulation, (c) the HC simulation (OHC-1) and (d) the simulated LGM–HC difference (OLGM-1 – OHC-1).

Earth system model simulations of the LGM

R. J. Matear et al.

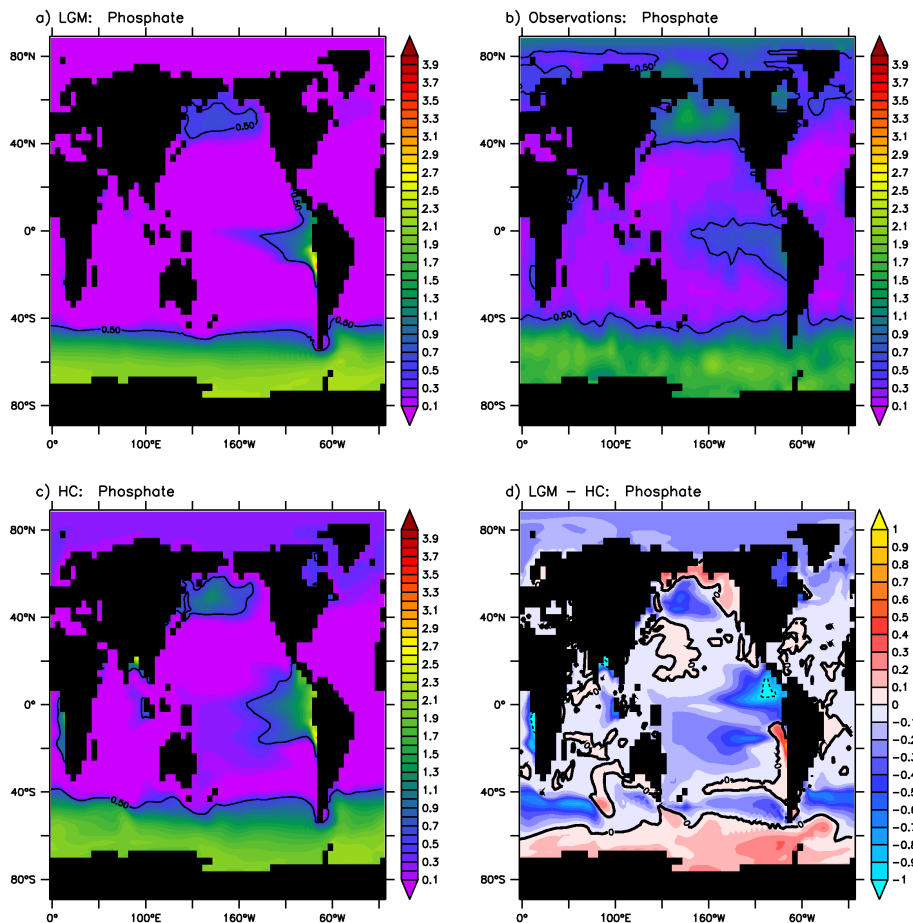


Figure 10. Annual mean phosphate concentration at 25 m (mmol m^{-3}) for **(a)** the LGM simulation (OLGM-1), **(b)** the observations from Garcia et al. (2006a), **(c)** the HC simulation (OHC-1) and **(d)** the simulated LGM–HC difference (OLGM-1 – OHC-1).

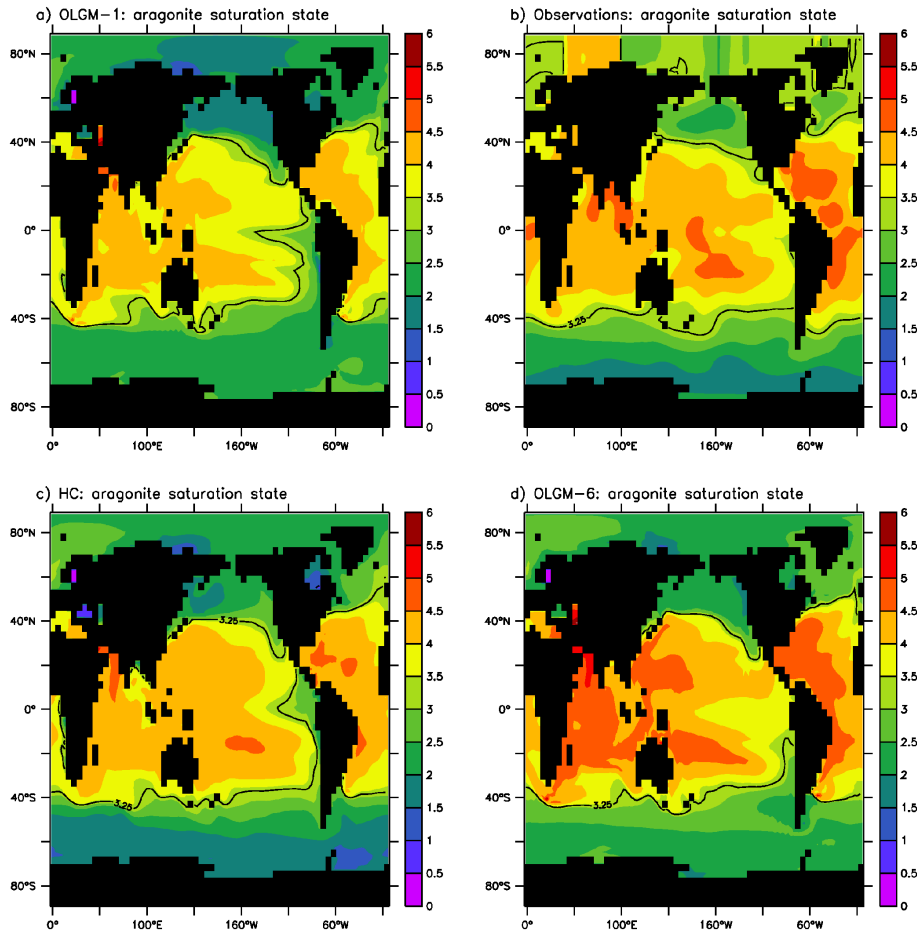


Figure 11. The annual average surface ocean aragonite saturation state for **(a)** the LGM simulation (OLGM-1), **(b)** calculated from the observations of Key et al. (2004), **(c)** the HC simulation (OHC-1) and **(d)** from the OLGM-6 simulation that used the modified BGC parameterizations.

Earth system model simulations of the LGM

R. J. Matear et al.

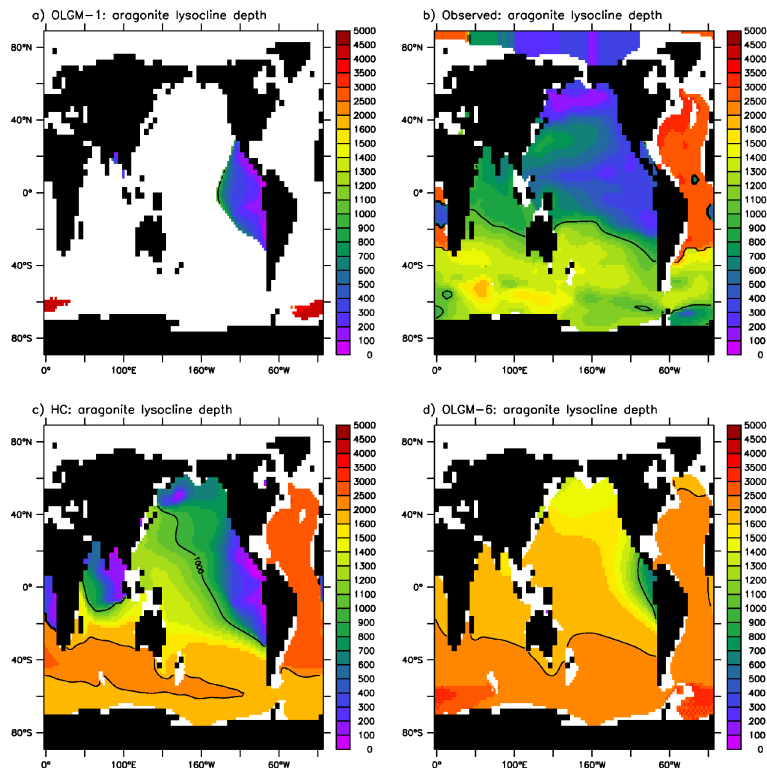


Figure 12. The depth where the aragonite saturation state equals one for (a) the LGM simulation (OLGM-1), (b) calculated from the observations of Key et al. (2004), (c) the HC simulation (OHC-1) and (d) the the OLG-6 simulation. The white areas in the ocean are regions where the lysocline is deeper than the ocean bottom.

Title Page

Abstract

Introduction

Conclusions

References

Tables

Figures



Back

Close

Full Screen / Esc

Printer-friendly Version

Interactive Discussion



Earth system model simulations of the LGM

R. J. Matear et al.

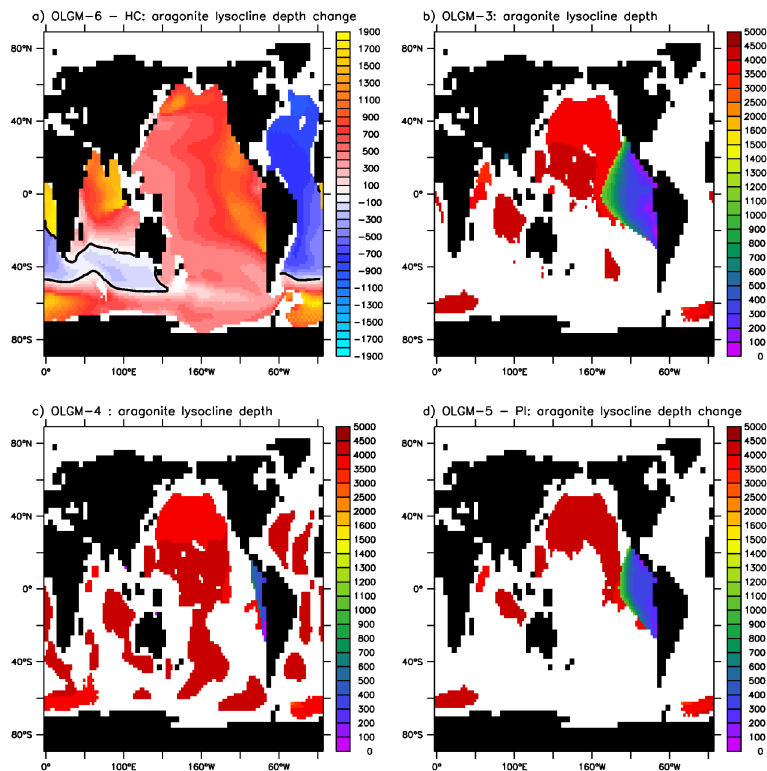


Figure 13. (a) Change in the depth where the aragonite saturation state equals one between modified BGC simulations (OLGM-6) and the HC simulation (OHC-1). The depth where the aragonite saturation state equals one for the (b) OLG-3, (c) OLG-4 and (d) OLG-5 simulations. The white areas in the ocean are regions where the lysocline is deeper than the ocean bottom.

Title Page

Abstract

Introduction

Conclusions

References

Tables

Figures



Back

Close

Full Screen / Esc

Printer-friendly Version

Interactive Discussion



Earth system model simulations of the LGM

R. J. Matear et al.

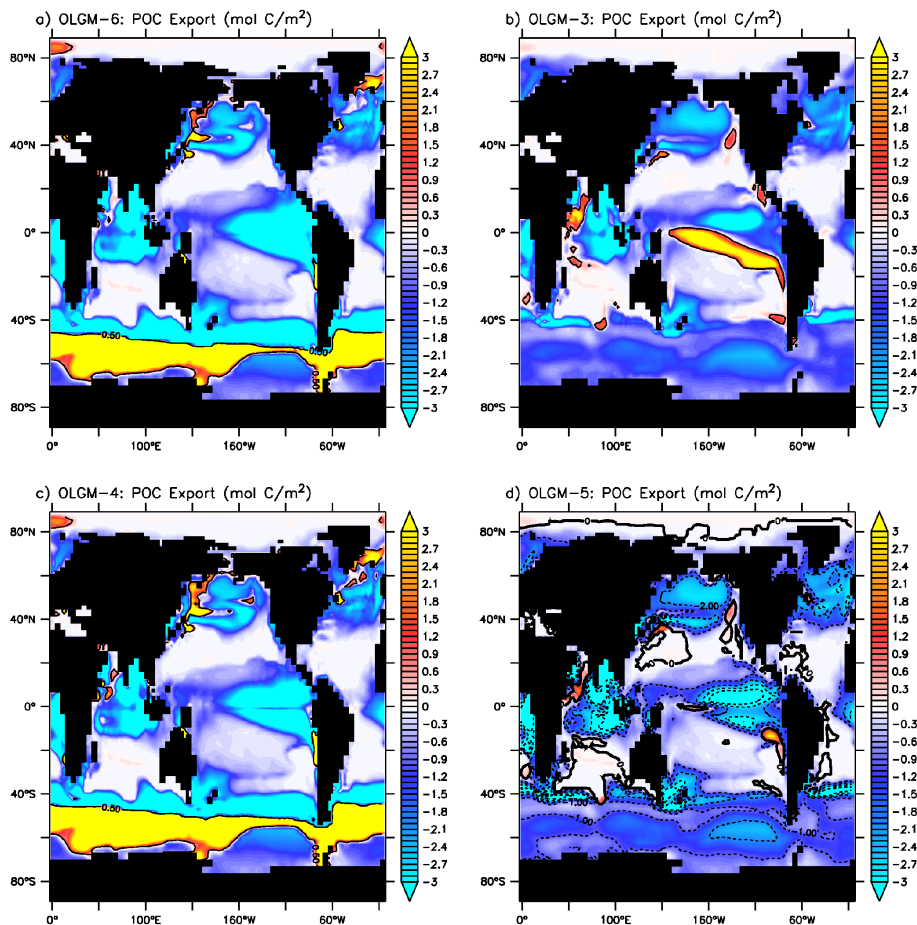


Figure 14. Change in annual export of particulate organic carbon from the upper 50 m ($\text{g C m}^{-2} \text{y}^{-1}$) between the LGM and HC from the simulations with modified BGC formulations for (a) OLG6-6 – OHC-1, (b) OLG6-3 – OHC-1, (c) OLG6-4 – OHC-1 and (d) OLG6-5 – OHC-1.

[Title Page](#)
[Abstract](#)
[Introduction](#)
[Conclusions](#)
[References](#)
[Tables](#)
[Figures](#)

[Back](#)
[Close](#)
[Full Screen / Esc](#)
[Printer-friendly Version](#)
[Interactive Discussion](#)


Earth system model simulations of the LGM

R. J. Matear et al.

Title Page

Abstract

Introduction

Conclusions

References

Tables

Figures



Back

Close

Full Screen / Esc

Printer-friendly Version

Interactive Discussion

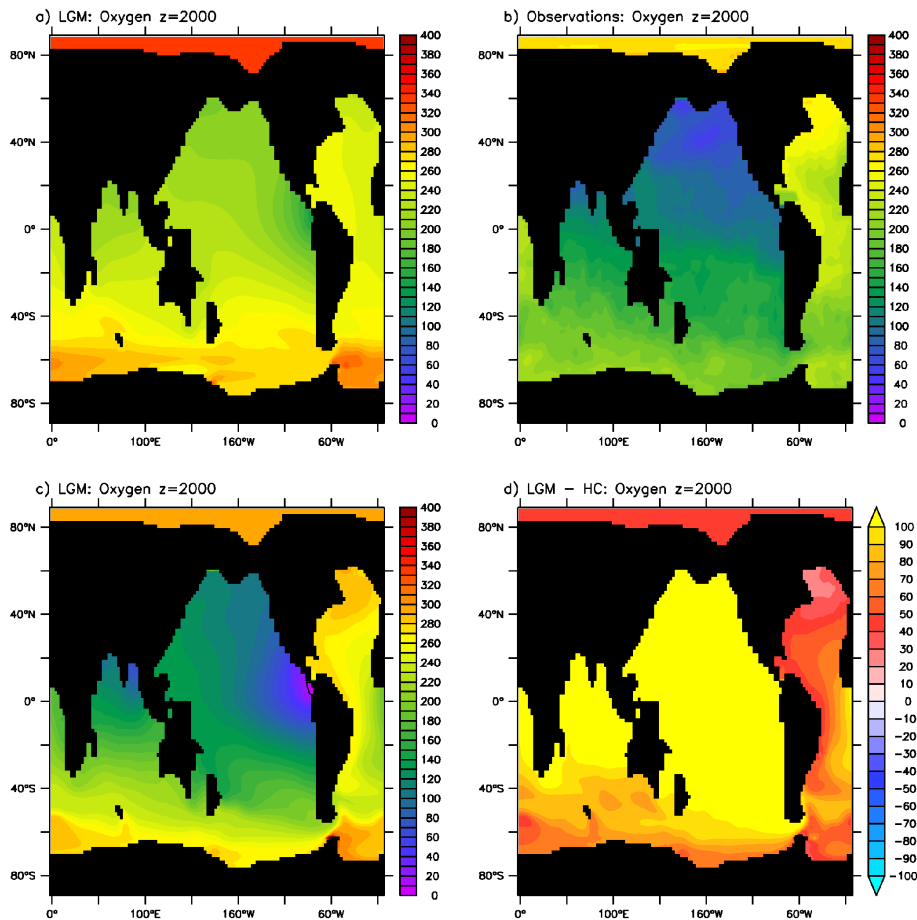


Figure 15. Averaged oxygen concentration (mmol m^{-3}) at 2000 m for **(a)** the LGM simulation (OLGM-1), **(b)** the observations from Garcia et al. (2006a), **(c)** the HC simulation (OHC-1) and **(d)** the simulated LGM–HC difference (OLGM-1 – OHC-1).

Earth system model simulations of the LGM

R. J. Matear et al.

Title Page

Abstract

Introduction

Conclusions

References

Tables

Figures



Back

Close

Full Screen / Esc

Printer-friendly Version

Interactive Discussion

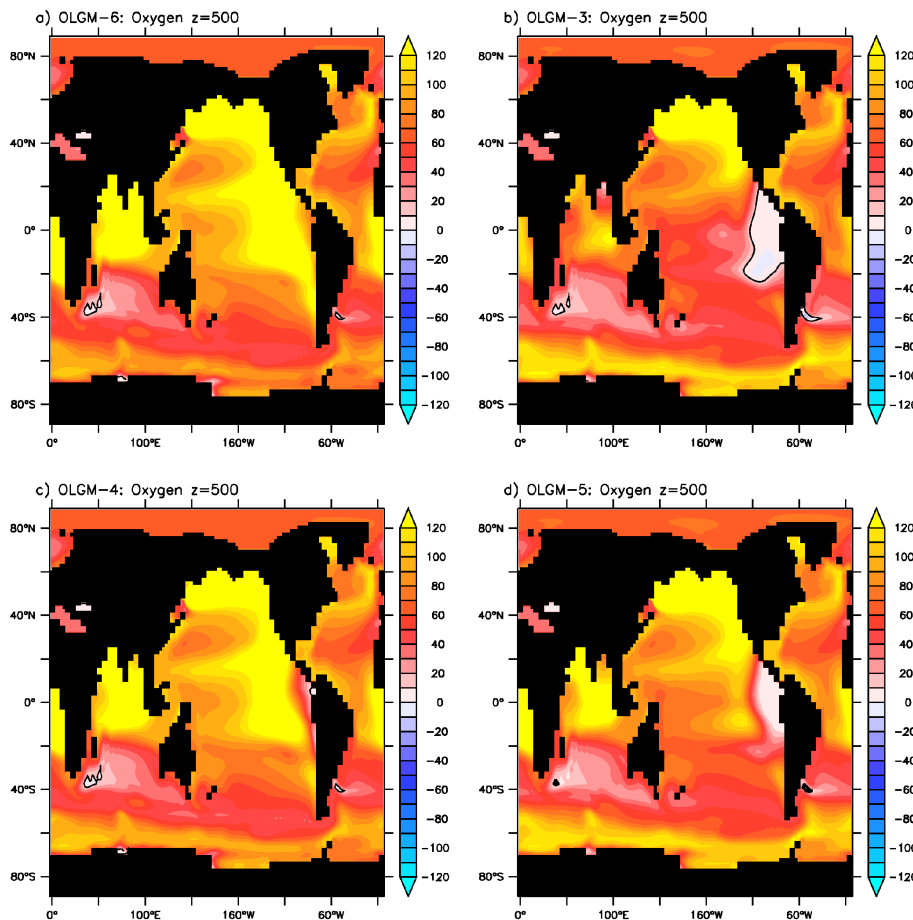


Figure 16. Change in oxygen concentration (mmol m^{-3}) at 500 m between the LGM and HC for (a) OLGM-6 – OHC-1, (b) OLGM-3 – OHC-1, (c) OLGM-4 – OHC-1 and (d) OLGM-5 – OHC-1.

Earth system model simulations of the LGM

R. J. Matear et al.

Title Page

Abstract

Introduction

Conclusions

References

Tables

Figures



Back

Close

Full Screen / Esc

Printer-friendly Version

Interactive Discussion

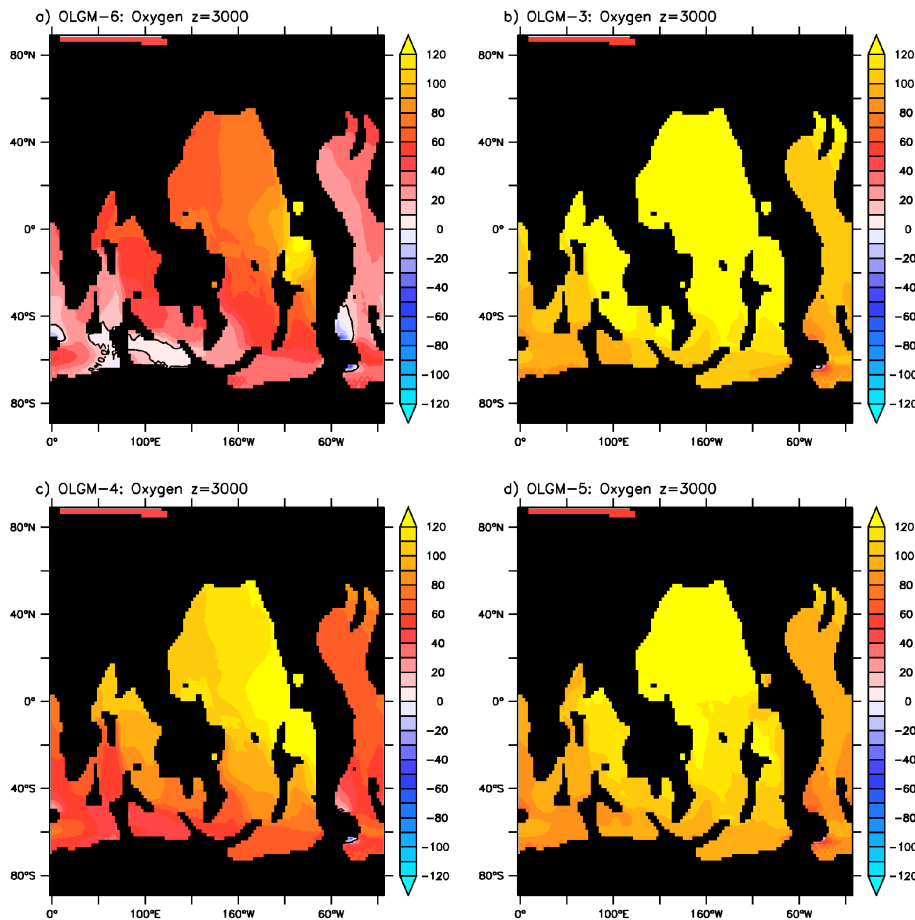


Figure 17. Change in oxygen concentration (mmol m^{-3}) at 3000m between the LGM and HC for (a) OLG-6 – OHC-1, (b) OLG-3 – OHC-1, (c) OLG-4 – OHC-1 and (d) OLG-5 – OHC-1.